JOURNAL OF THEORETICAL AND APPLIED MECHANICS
41, 4, pp. 789-803, Warsaw 2003

THE INVERSE PROBLEM IN A HYPERBOLIC-SECTION RADIAL COMPRESSOR

Romuald Puzyrewski
Paweł Flaszyński

Turbomachinery and Fluid Mechanics Faculty, Gdańsk University of Technology
e-mail: rpuzyrew@pg.gda.pl; pflaszyn@pg.gda.pl

A comparison between the inverse method, leading within the framework of the 2D model to prediction of the optimal rotor shape and the direct approach for evaluating flow through a preexisting rotor shape utilizing a 3D model is presented in this paper. The principle of shaping the rotor envelope and blading within the 2D model is illustrated, followed by subsequent computation of 3D flow through the resulting model. The design goal is to obtain uniform distributions of flow parameters within the rotor while avoiding separated flow. It is also shown how the altering of the overall shape of the rotor from conical to hyperboloidal affects the uniformity of velocity distribution upstream of the rotor inlet.

Key words: compressor, inverse problem, 2D model

Important symbols

e_0	–	total energy
f	–	shape function of stream surface S_2
$f_{x_1}, f_{x_2}, f_{x_3}$	–	body force components
p	–	pressure
T	–	temperature
U_{x_2}, U_{x_3}	–	velocity components
x_1, x_2, x_3	–	curvlinear coordinates
ζ	–	isentropic loss coefficient
τ	–	flow-area reduction factor

1. Introduction

The evolution of the outline of the compressor stage is shown in Fig. 1, according to publications by Siemens company (Tosza and Magdalinski, 2002).

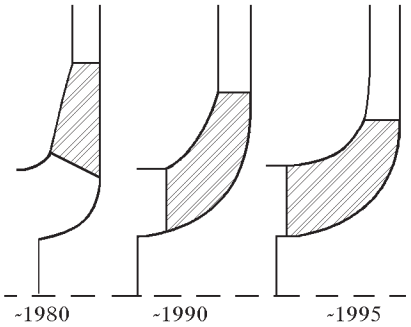

Fig. 1. Evolution of compressor meridional shape

As may be observed, strict radial shape delimited by straight lines has gradually evolved towards a curved hyperbola-delimited cross-section, with marked tendency toward reducing the diameter and extending the blade in the axial direction. The present work can serve to illustrate this progress from the traditional cone-bounded rotor towards the hyperboloid-of-revolution-bounded rotor. The starting point is the rotor shape illustrated in Fig. 2, for which 3D computations have been carried out. The results have shown a distinct region of separated flow localized at the inlet (Fig. 3.).

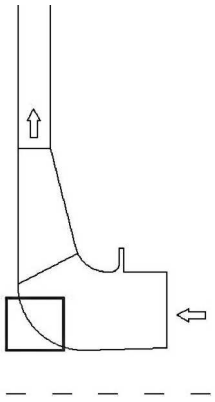

Fig. 2. Radial compressor (meridional section)

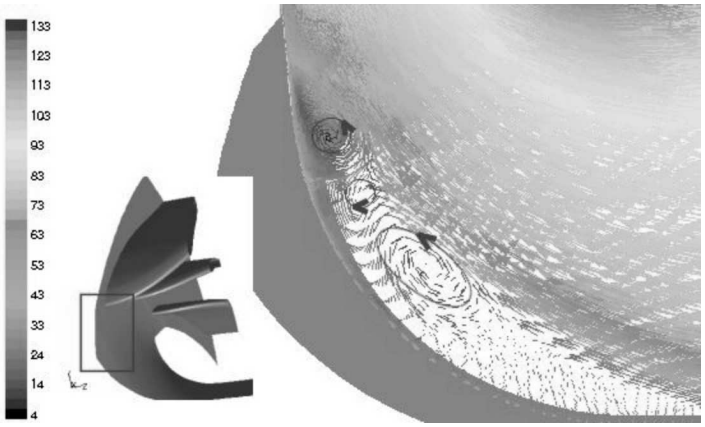

Fig. 3. Separation zone upstream to the leading edge

Three distinct vortices can be made out in Fig. 3, which indicates that the primary vortex is of intensity high enough to generate and feed the subsequent two vortices. The large extent of the separation-affected region is also quite noticeable. There are two incentives that make the elimination of this region desirable. Firstly, unwanted dissipation effects are invariably exacerbated through the presence of separation zones. Secondly, the existing separation adversely affects the uniformity of flow distribution at the entrance to the rotor. Such non-uniform inflow requires complex special modifications of blade shape; if such design modifications are not made and the flow is treated as uniform, additional losses will be incurred within the rotor.

2. Hyperbolic outline of rotor cross-section

The cross-section outline of the modified rotor is shown in Fig. 4. The casing has the form of a hyperboloid of revolution generated by the hyperbola

$$f_d = d_1 + d_2 x_3^{-n_d} \tag{2.1}$$

The particular hyperbola was chosen so as to avoid the occurrence of separation similar to that shown in Fig. 3. The remaining curves enclosing the rotor cross-section are described analytically by the equations

$$f_b = b_1 + b_2 x_3^{-n_b} \qquad f_{inl} = a + bx_3 \qquad f_{out} = r_k \tag{2.2}$$

Thus, the configuration of the rotor envelope is fully described by nine parameters: d_1, d_2, n_d, b_1, b_2, n_b, a, b, r_k. The parameters d_1, d_2, n_d have been chosen so as to eliminate the separated region where the flow is turned from the axial to radial direction. The resulting line is characterized by continuous curvature, as opposed to the conventional jump in the curvature at the juncture of the straight line and arc (Fig. 2). The parameters b_1, b_2, a, b follow from the choice of the points P_2, R_1, R_2, as shown in Fig. 5; these points, as well as the quantity r_k, follow in turn from the assumed dimensions of the compressor stage. The remaining free parameter n_b can be obtained by stating the requirement of uniform flow parameter distribution at the outlet from the rotor, along the line P_1 - P_2. With this end in mind, let us define the following family of curves

$$f = f(x_1, x_3) = x_1 f_b + (1 - x_1) f_d \tag{2.3}$$

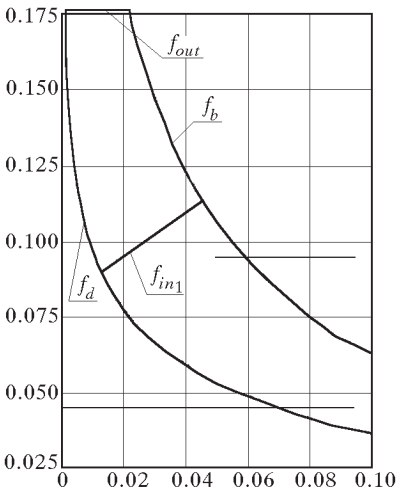

Fig. 4. Blade channel boundaries

Note that with $x_1 = 0$ one obtains the profile of the hub disc, and with $x_1 = 1$ the profile of the outer casing. The curves $x_1 = \text{const}$ follow the pattern shown in Fig. 5, forming the basis of a family of hyperboloids of revolution which can be used as the basis for defining the curvilinear coordinate system (x_1, x_2, x_3).

The conversion rule with regard to the cartesian system can be written as

$$x = f(x_1, x_3)\cos x_2 \qquad y = f(x_1, x_3)\cos x_2 \qquad z = x_3 \tag{2.4}$$

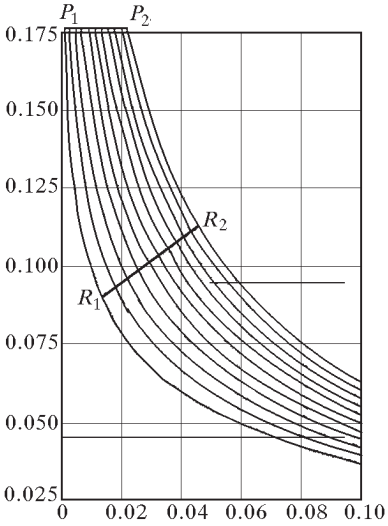

Fig. 5. Streamsurfaces S_1 in meridional cross-section

If the surfaces $x_1 = \text{const}$ are taken as stream surfaces, then the problem of designing the corresponding blade configuration within the $R_1R_2P_2P_1$ region reduces to the solution of the following system of equations:

- the mass conservation (continuity) equation

$$[1-\tau(x_1,x_3)]\rho U_{x_3}\frac{f\frac{\partial f}{\partial x_1}}{\sqrt{1+\left(\frac{\partial f}{\partial x_3}\right)^2}} = m(x_1) \tag{2.5}$$

- momentum conservation equations:
  - in the x_1 direction

$$-\frac{\rho U_{x_2}^2}{f} + \frac{\rho U_{x_3}^2\frac{\partial^2 f}{\partial x_3^2}}{1+\left(\frac{\partial f}{\partial x_3}\right)^2} = -\frac{\partial p}{\partial x_1}\frac{1+\left(\frac{\partial f}{\partial x_3}\right)^2}{\frac{\partial f}{\partial x_1}} + \frac{\partial p}{\partial x_3}\frac{\partial f}{\partial x_3} + \rho f_{x_1} \tag{2.6}$$

  - in the x_2 direction

$$\frac{\rho U_{x_3}}{f\sqrt{1+\left(\frac{\partial f}{\partial x_3}\right)^2}}\frac{\partial(fU_{x_3})}{\partial x_3} = \rho f_{x_2} \tag{2.7}$$

– in the x_3 direction

$$\frac{\rho U_{x_3}}{\sqrt{1+\left(\frac{\partial f}{\partial x_3}\right)^2}}\left(\frac{\partial U_{x_3}}{\partial x_3}-\frac{U_{x_3}}{1+\left(\frac{\partial f}{\partial x_3}\right)^2}\frac{\partial f}{\partial x_3}\frac{\partial^2 f}{\partial x_3^2}\right)= \\ =\frac{\partial p}{\partial x_1}\frac{\frac{\partial f}{\partial x_3}}{\frac{\partial f}{\partial x_1}}\sqrt{1+\left(\frac{\partial f}{\partial x_3}\right)^2}-\frac{\partial p}{\partial x_3}\sqrt{1+\left(\frac{\partial f}{\partial x_3}\right)^2}+\rho f_{x_3} \tag{2.8}$$

- the energy conservation equation (u_r-rotor velocity)

$$\frac{U_{x_2}^2+U_{x_3}^2}{2}-u_r U_{x_2}+\frac{k}{k-1}\frac{p}{\rho}=e_0(x_1) \tag{2.9}$$

- the process equation (an integral of the Gibbs equation with the definition of the loss coefficient)

$$\rho=\rho_1\Big(\frac{p}{p_1}\Big)^{\frac{1}{k}}\exp\left[\frac{\zeta\Big[\Big(\frac{p_1}{p}\Big)^{\frac{k-1}{k}}-1\Big]}{\sqrt{(1-\zeta)\Big[1-\zeta\Big(\frac{p_1}{p}\Big)^{\frac{k-1}{k}}\Big]}}\right] \tag{2.10}$$

This system of 6 equations, however, contains 9 unknowns

$$U_{x_2},\ U_{x_3},\ f_{x_1},\ f_{x_2},\ f_{x_3},\ \rho,\ p,\ \tau,\ \zeta$$

Its closure thus calls for additional assumptions with regard to three of the above quantities. Let us focus for the moment on continuity equation (2.5). Transforming it, one obtains the formula

$$\rho U_{x_3}=\frac{m(x_1)}{[1-\tau(x_1,x_3)]\frac{f\frac{\partial f}{\partial x_1}}{\sqrt{1+\left(\frac{\partial f}{\partial x_3}\right)^2}}}=\frac{m(x_1)}{[1-\tau(x_1,x_3)]P_u(x_1,x_3)} \tag{2.11}$$

where the parameter P_u depends solely on the geometric configuration

$$P_u(x_1,x_3)=\frac{f\frac{\partial f}{\partial x_1}}{\sqrt{1+\left(\frac{\partial f}{\partial x_3}\right)^2}} \tag{2.12}$$

If one were to aim at uniformity of ρU_{x_3} distribution at the outlet stage, then all the functions taking part in relation (2.11) should approach constant

values. The function $m(x_1)$ is dependent on conditions at the outlet stage (line P_1 - P_2). Any non-uniformity with regard to the parameters making up $m(x_1)$ is reflected in a corresponding non-uniformity at the outlet. This can be compensated by varying P_u. Let us introduce a quantitative measure of the non-uniformity in the parameter P_u, based on deviation from the mean value

$$m_{P_u} = \frac{1}{x_{3R_2} - x_{3P_2}} \int_{x_3P_2}^{x_3R_2} P_u \, dx_3 \tag{2.13}$$

The non-uniformity factor can be then expressed as follows

$$N_{Pu} = \frac{1}{m_{p_u}} \sqrt{\frac{1}{x_{3R_2} - x_{3P_2}} \int_{x_3P_2}^{x_3R_2} (P_u - m_{Pu})^2 \, dx_3} \tag{2.14}$$

In relation (2.12) for the outlet, the coordinate x_1 can be eliminated by making use of the formula

$$x_1 = \frac{r_k - f_d}{f_b - f_d} \tag{2.15}$$

where the expressions

$$\begin{aligned} r_{P_2} &= r_k = b_1 + b_2 x_{3P_2}^{-n_b} \\ r_{R_2} &= r_k = b_1 + b_2 x_{3R_2}^{-n_b} \end{aligned} \tag{2.16}$$

serve to determine the parameters b_1, b_2. Thus, the parameter P_u becomes a function of the arguments (x_3, b_1, b_2, n_b) only, while N_{P_u} is the function of n_b alone. For actual values of all remaining parameters as listed below

$$\begin{aligned} d_1 &= 0.195789 \quad r_k = 0.176 \\ d_2 &= 0.186336 \quad a = 0.0900253 \\ n_d &= 0.1 \qquad\quad b = 0.472992 \end{aligned} \tag{2.17}$$

the non-uniformity factor N_{P_u} varies with n_b as shown in Fig. 6.

It should be noted that the minimum of N_{P_u} falls in the vicinity of 0.50 - 0.55. The values of the remaining parameters are summarized in Table 1.

Table 1

n_b	b_1	b_2	N_f
0.45	−0.05020536	0.040771974	0.035485
0.50	−0.03115712	0.030865716	0.012092
0.55	−0.01560754	0.023599713	0.019275
0.60	−0.00268185	0.018192493	0.047338

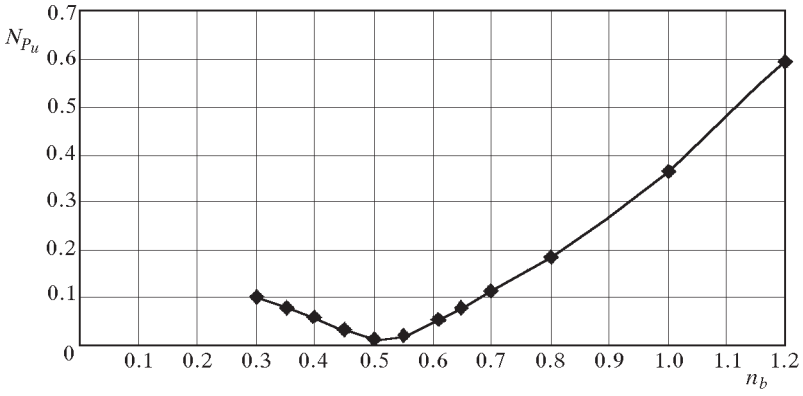

Fig. 6. Non-uniformity factor N_{P_u}

The behavior of the parameter $P_u = P_u(x_3)$ at the outlet is illustrated in Fig. 7 for $n_b = 0.5$. This is the value for which N_{P_u} reaches its minimum of approximately $N_{P_u} \approx 0.012$.

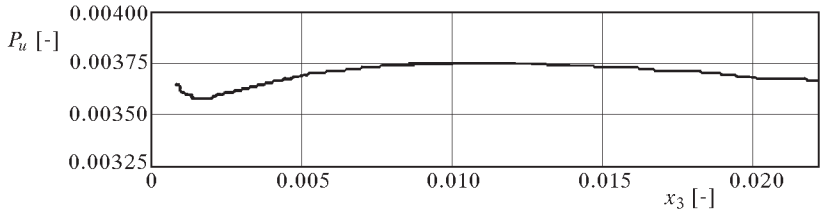

Fig. 7. Parameter P_u as function of x_3

3. Results of 3D calculations for the hyperboloid-walled rotor

Solving the above system of equations describing the 2D model yields the shape of the rotor blade surface. The solution uses additional closing assumptions in the form of the following relations describing the loss coefficient within the rotor region (r, x_1)

$$r_1 = \frac{r - r_{in_1}}{r_k - r_{in_1}}$$
$$\zeta = [w_0 r_1 + (1 - w_0) r_1^{n_0}][w_1 + w_2(1 - x_1)^{n_1}] + w_3 x_1^{n_2} \tag{3.1}$$

with the constants set to

$$\begin{aligned} &w_0 = 0.5 \quad w_1 = 0.05 \quad w_2 = 0.0 \quad w_3 = 0.0 \\ &n_0 = 15 \quad\;\; n_1 = 40 \quad\;\; n_2 = 30 \end{aligned} \tag{3.2}$$

so that the level of losses should closely mimic what can be expected in the rotor region. Two additional functions $\tau(x_1, x_3) = 0$ and $fx_1 = 0$ were formulated. These are preliminary simplifications which can be prospectively replaced by other closure functions matching better the expected values, of fx_1 in particular.

The resulting surface is shown in Fig. 8. After allowing for the profile thickness (approx. 5 mm) the blade can be modelled along it. The curves making up the surface are fluid element trajectories passing along axisymmetric stream surfaces described by the function f as defined in relation (2.3).

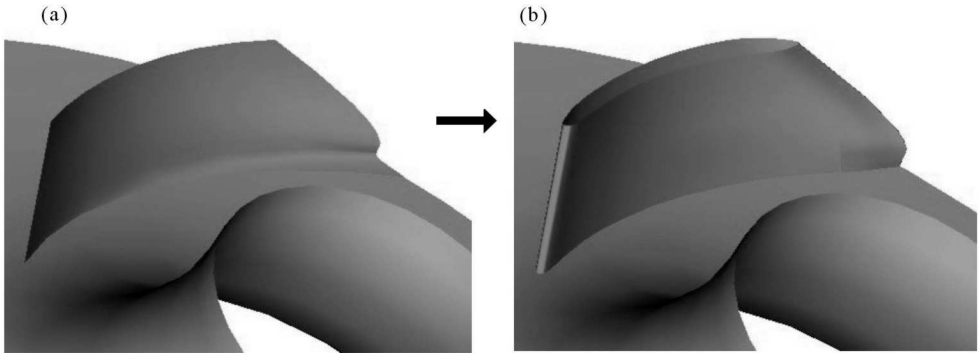

Fig. 8. Stream surface S_2 (a) and final blade shape (b)

The following illustrations compare the calculation results from the 2D and 3D models. The boundary conditions for the 3D model are as formulated by Flaszyński and Puzyrewski (2001). Figure 9 shows the distribution of static pressure at the inlet to the bladed region of the rotor. Figure 10 shows the corresponding velocity distribution, and Fig. 11 the distribution of pressure at the rotor disc from the inlet to outlet.

As may be observed, the principal effect of passing into the three-dimensional regimen is manifested by noticeably lower pressure ratio along the disc, as seen in Fig. 11. This effect is likewise evident in Fig. 12 and Fig. 13. As it turns out, the outlet angle in the 3D calculations differs from the 2D results by some 6°. This, in turn, influences the velocity distribution at the outlet (Fig. 13). All these effects must be taken into account in the design process, if the 2D inverse method is to be used to its full potential. Specifically,

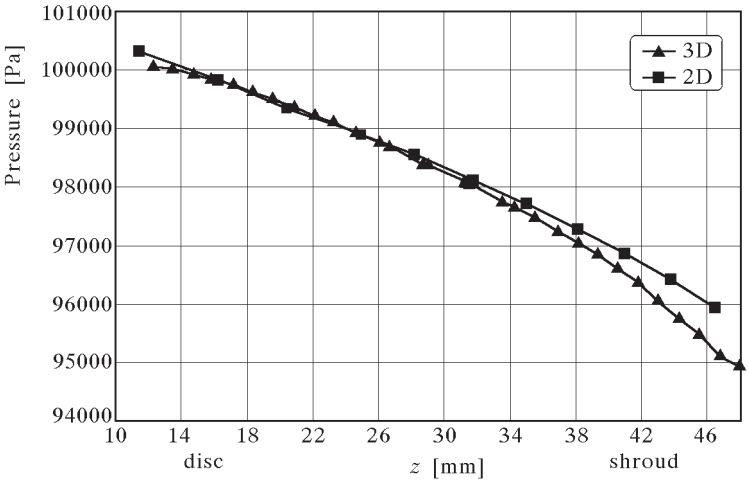

Fig. 9. Pressure distribution at the inlet section

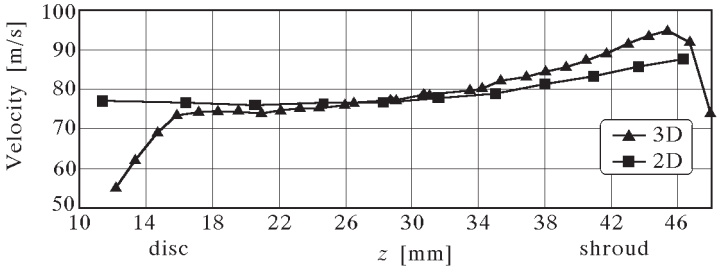

Fig. 10. Velocity distribution at the inlet section

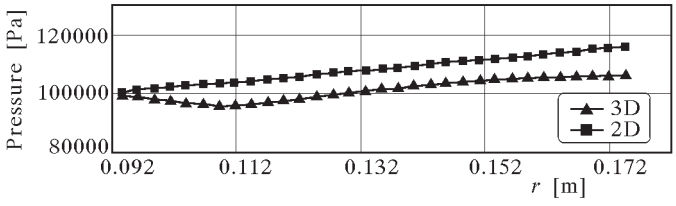

Fig. 11. Pressure distribution along the disc

in anticipation of these minor discrepancies due to 3D effects, the designer should specify a slightly higher pressure ratio, while realizing that the outlet angle obtained from a finite number of blades is likely to be lower than the theoretically obtained value.

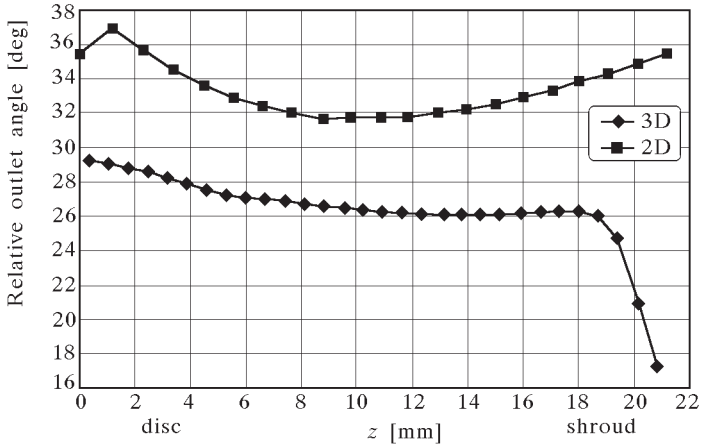

Fig. 12. Velocity angle at the impeller outlet

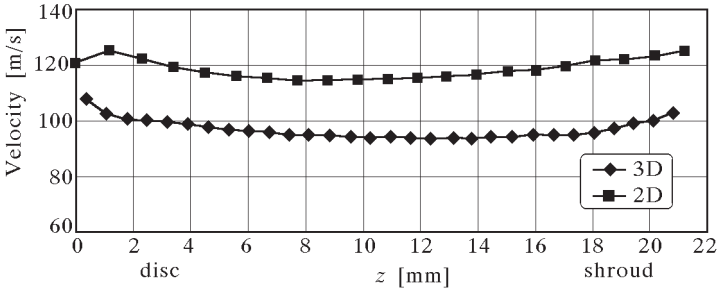

Fig. 13. Velocity at the impeller outlet

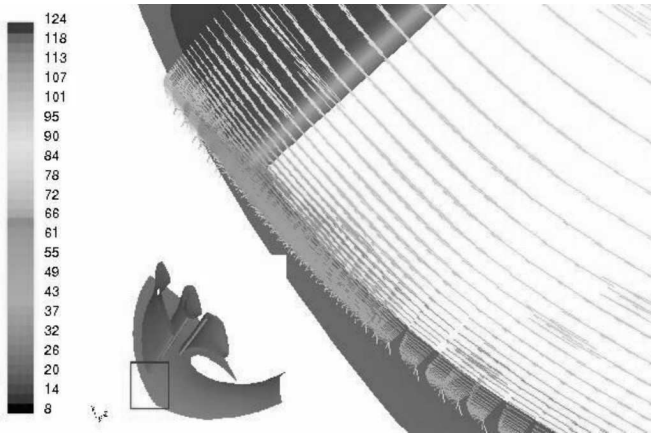

Fig. 14. Velocity vectors close to the disc upstream the leading edge

On the other hand, it is encouraging to note that the qualitative pattern of parameter variation exhibits close correspondence between the 2D and 3D models.

A major improvement with regard to the existing design is evident with regard to the velocity distribution at the inlet, where the extensive separation zone has been entirely eliminated, as shown in Fig. 14. This translates to a marked improvement in the flow conditions at the inlet to the blading region.

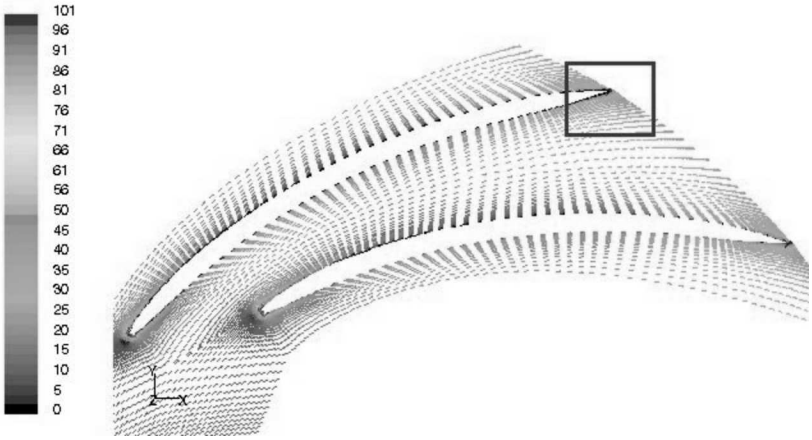

Fig. 15. Velocity vectors close to the disc

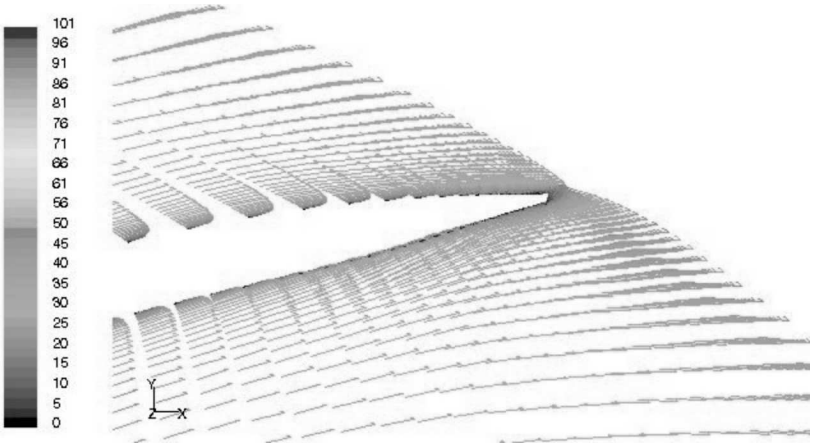

Fig. 16. Velocity vectors in the vicinity of the trailing edge

Figures 15 and 16 illustrate the velocity distributions in the neighborhood of the rotor disc. Again, no separation zones are noted, in contrast to what is typical for the majority of existing compressors.

Figures 17 and 18 show the corresponding velocity patterns in the vicinity of the cover plate. Here the extensive separation zones are absent as well. At the trailing edge a small separation region occurs, but it is caused by the abrupt profiling of the trailing edge.

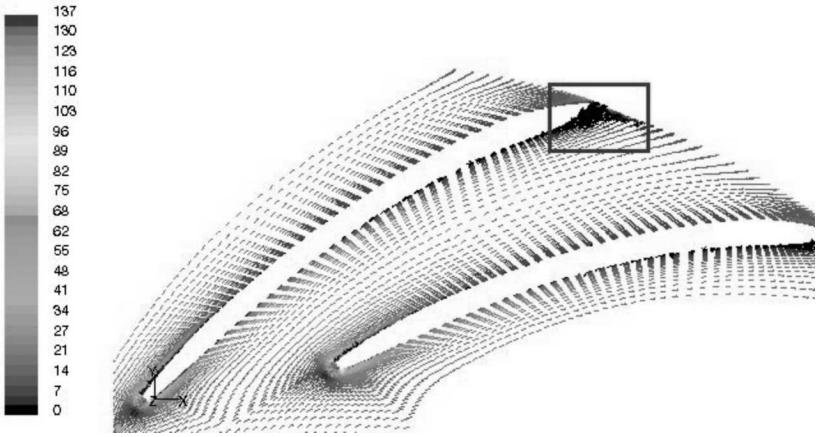

Fig. 17. Velocity vectors close to the shroud

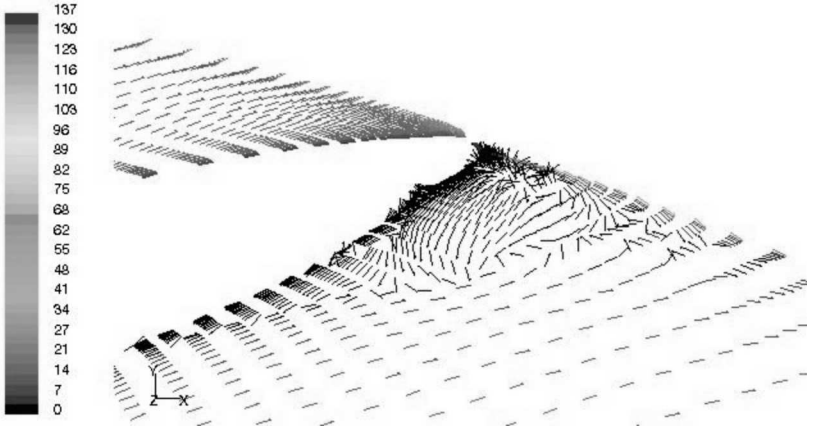

Fig. 18. Velocity vectors in the vicinity of the trailing edge

4. Conclusions

The design method presented in this paper has made it possible to uniformize substantially the velocity field within the blading of a compressor. It still remains to optimize the flow with regard to the dissipative losses generated at the washed surfaces as well as within the recirculation zones.

Acknowledgment

The research for this paper has been carried out as a part of the State Committee for Scientific Research (KBN) project No. 8T10B 00419.

References

1. FLASZYŃSKI P., PUZYREWSKI R., 2001, *Obliczenia 3D (FLUENT) dla różnych modeli turbulencji. Analiza wyników. Wnioski*, Projekt KBN 8T10B 00419, Etap 6, Gdańsk, September
2. PUZYREWSKI R., 1998, *14 wykładów teorii stopnia maszyny wirnikowej – model dwuwymiarowy (3D)*, Wydawnictwo Politechniki Gdańskiej, Gdańsk
3. PUZYREWSKI R., FLASZYŃSKI P., 2001, *Projekt wirnika metodą zadania odwrotnego 2D*, Projekt KBN 8T10B 00419, Etap 7, Gdańsk
4. PUZYREWSKI R., FLASZYŃSKI P., 2002, *Modyfikacja I (pierwsza) kształtu wirnika w strefie oderwań. (Sprawdzenie efektów obliczeniami)*, Projekt KBN 8T10B 00419, Etap 10, Gdańsk
5. TOSZA T., MAGDALINSKI CH., 2002, Modernizaciya kompressorov. Vozmozhnosti i koniechnye rezultaty adaptacii rabochikh kharakteristik kompressora k izmeneniyu uslowiĭ, *Mezhdunarodniĭ Sympozyum "Potrebitieli-Proizvoditeli kompressorow i kompressornogo oborudovaniya"*, Sankt Peterburg Izdatelstvo SP GTU

Zadanie odwrotne dla sprężarki promieniowej o hiperbolicznym kształcie

Streszczenie

Porównano rozwiązanie zadania odwrotnego w ramach modelu dwuwymiarowego, prowadzącego do kształtu koła wirnikowego, z zadaniem prostym rozwiązanym w ramach modelu trójwymiarowego dla skonstruowanego wirnika. Przedstawiono elementy algorytmu kształtowania łopatek przy wykorzystaniu modelu dwuwymiarowego.

W podanym przykładzie wskazano możliwość optymalizacji kształtu jednego z ograniczeń kanału w celu uzyskania równomiernego rozkładu parametrów w przekroju wylotowym. Pokazano jak zmiana obrysu wirnika z klasycznego kształtu stożkowego na hiperboliczny może wpłynąć na równomierność rozkładu pól prędkości przed układem łopatkowym.

Manuscript received November 21, 2002; accepted for print February 27, 2003